Origin of crystalline silicates from Comet 81P/Wild 2: Combined study on their oxygen isotopes and mineral chemistry

Céline Defouilloy[a,*], Daisuke Nakashima[b], David J. Joswiak[c], Donald E. Brownlee[c], Travis J. Tenner[a,†], Noriko T. Kita[a]

[a]WiscSIMS, Department of Geoscience, University of Wisconsin-Madison, Madison, WI 53706, USA.

[b]Division of Earth and Planetary Materials Science, Tohoku University, Miyagi 980-8578, Japan.

[c]Department of Astronomy, University of Washington, Seattle, WA 98195, USA.

*corresponding author: defouilloy@wisc.edu

[†]Current address: Chemistry Division, Nuclear and Radiochemistry, Los Alamos National Laboratory, MSJ514 Los Alamos, NM 87545, USA

Highlights:

► 7 silicates grains from comet Wild 2 were analyzed for their oxygen isotope ratios.

► ^{16}O-poor particles show Δ^{17}O-Mg# range and variations similar to CR chondrites.

► We found the first ^{16}O-rich pyroxenes.

► ^{16}O-rich pyroxenes show similarities with AOAs enstatites and are likely condensates.

Keywords: oxygen isotope ratios; crystalline silicate; comet 81P/Wild 2; solar system formation; Stardust

Abstract

In order to explore the link between comet 81P/Wild 2 and materials in primitive meteorites, seven particles 5 to 15 μm in diameter from comet 81P/Wild 2 have been analyzed for their oxygen isotope ratios using a secondary ion mass spectrometer. Most particles are single minerals consisting of olivine or pyroxene with Mg# higher than 85, which are relatively minor in 81P/Wild 2 particles (~1/3 of the ^{16}O-poor cluster). Four particles extracted from Track 149 are ^{16}O-poor and show $\Delta^{17}O$ (= $\delta^{17}O - 0.52 \times \delta^{18}O$) values from –2‰ to +1‰, similar to previous studies, while one enstatite (En_{99}) particle shows lower $\Delta^{17}O$ value of –7±4‰ (2σ). This compositional range has not been reported among ^{16}O-poor particles in 81P/Wild 2, but is commonly observed among chondrules in carbonaceous chondrites and in particular in CR chondrites. The distribution in $\Delta^{17}O$ indicates that ^{16}O-poor 81P/Wild 2 particles are most similar to chondrules (and their fragments) in the CR chondrites and Tagish Lake-like WIS91600 chondrite chondrule silicate grains, which indicates that they likely come from a reservoir with similar dust/ice ratios as CR chondrites and WIS91600. However, differences in the Mg# distribution imply that the 81P/Wild 2 reservoir was comparatively more oxidized, with a higher dust enrichment. Two nearly pure enstatite grains from track 172 are significantly enriched in ^{16}O, with $\delta^{18}O$ values of –51.2 ± 1.5‰ (2σ) and –43.0 ± 1.3‰ (2σ), respectively, and $\Delta^{17}O$ values of –22.3 ± 1.9‰ (2σ) and –21.3 ± 2.3‰ (2σ), respectively. They are the first ^{16}O-rich pyroxenes found among 81P/Wild 2 particles, with similar $\Delta^{17}O$ values to those of ^{16}O-rich low-iron, manganese-enriched (LIME) olivine and CAI (calcium and aluminum-rich inclusions) -like particles from 81P/Wild 2. The major element and oxygen isotopic compositions of the pyroxenes are similar to those of enstatite in amoeboid olivine aggregates (AOAs) in primitive chondrites, in which ^{16}O-rich pyroxenes have previously been found, and thus suggest a condensation origin.

1. Introduction

In 2006, the Stardust spacecraft returned to Earth a precious cargo of comet particles collected during a close fly-by of the Jupiter Family Comet (JFC) 81P/Wild 2. Expectations were that the particles, coming from cold regions of the Solar System, would provide new insights on the characteristics of the outer solar system and would predominantly be composed of presolar interstellar grains (Greenberg and Li, 1999). However, close examination of the returned samples revealed an unexpected assemblages. If a few presolar grains (Messenger et al., 2009; Leitner et al., 2010) and organic matter (Sandford et al., 2006; Matrajt et al., 2008) were found, the majority of the collected particles resembled chondritic materials. Numerous high-temperature materials were collected, such as Ca, Al-rich inclusions (CAIs; e.g. Zolensky et al., 2006; Joswiak et al., 2012) and ferromagnesian chondrule fragments (Nakamura et al., 2008; Gainsforth et al., 2015; Bridges et al., 2012; Joswiak et al., 2012; Nakashima et al., 2012; Ogliore et al., 2012).

The oxygen isotope ratios of 81P/Wild 2 particles span a large range in delta notation (where $\delta^{17,18}O = [(R_{sample}/R_{VSMOW}) - 1] \times 1000$; $R = {}^{17,18}O/{}^{16}O$; and VSMOW = Vienna Standard Mean Ocean Water). $\delta^{18}O$ and $\delta^{17}O$ values of >2 μm crystalline particles vary from –55‰ to +6‰, and $\Delta^{17}O$ ($= \delta^{17}O - 0.52 \times \delta^{18}O$) varies from –27‰ to +2.5‰ (McKeegan et al., 2006; Nakamura et al., 2008; Nakamura-Messenger et al., 2011; Bridges et al., 2012; Ogliore et al., 2012, 2015; Nakashima et al., 2012; Joswiak et al., 2014; Gainsforth et al., 2015). Particles smaller than 2 μm show even larger variations, with $\Delta^{17}O$ ranging from –80‰ to +60‰ (Ogliore et al., 2015). All 81P/Wild 2 data plot on a slope ~1 mixing line when comparing $\delta^{17}O$ vs. $\delta^{18}O$, similar to CCAM (Carbonaceous Chondrite Anhydrous Minerals; Clayton et al., 1977) or PCM (Primitive

Chondrule Minerals; Ushikubo et al., 2012) lines. In a 3 oxygen isotope plot ($\delta^{17}O$ vs. $\delta^{18}O$), >2 μm particles form two clusters of data. The first one, representing ^{16}O-poor chondrule-like minerals, shows $\Delta^{17}O$ values of –5‰ to + 2.5‰. The second cluster varies from $\Delta^{17}O$ = –24‰ to –20‰ and is composed of CAI-like particles, LIME (low-iron, manganese-enriched) olivines and relict olivine grains in the chondrule-like objects (McKeegan et al., 2006; Nakamura et al., 2008; Nakashima et al., 2012).

The redox environment during the formation of crystalline silicate particles can be examined by the Mg# (mol% MgO/[MgO + FeO]) of olivine and pyroxene, which is related to the amount of iron distributed between metal and oxide (FeO) incorporated into the silicate grains (e.g., Tenner et al. 2015). In primitive chondrites, the Mg# of olivine and pyroxene in chondrules varies from 40 to 100 (Connolly Jr. and Huss, 2010; Kita et al., 2010; Rudraswami et al., 2011; Ushikubo et al., 2012; Schrader et al., 2013; Tenner et al., 2013, 2015). Based on their constituent olivine and/or pyroxene Mg#'s, chondrules are sorted into two groups: type I chondrules (FeO-poor, reduced), which have Mg#'s between 90 and 100, and type II chondrules (FeO-rich, oxidized) with Mg#'s < 90. The composition of 81P/Wild 2 silicate grains covers a similar range of Mg# as silicates found in various chondrite chondrules, though chondrules contain more grains with type I characteristics (Frank et al., 2014). Studies have shown distinctive Mg#-$\Delta^{17}O$ trends between different groups of chondrite chondrules (Connolly Jr. and Huss, 2010; Kita et al., 2010; Weisberg et al., 2011; Nakashima et al., 2012; Ushikubo et al., 2012; Schrader et al., 2013; Tenner et al., 2013, 2015). In ordinary and enstatite chondrites, $\Delta^{17}O$ values of chondrules are mostly zero or positive and are constant as a function of Mg#. In contrast, chondrules from carbonaceous chondrites show mostly negative $\Delta^{17}O$ values that show group specific correlations with Mg#. In CR chondrite chondrules, $\Delta^{17}O$ values of type I chondrules increase with decreasing Mg# from –

6‰ to ~0 ‰ (Tenner et al., 2015). This has been explained by the addition of water ice with positive $\Delta^{17}O$ values as an oxidant to anhydrous dust with a $\Delta^{17}O$ value ~ –6‰. Tenner et al. (2015) hypothesized that chondrules with the highest Mg#'s (≥98) and $\Delta^{17}O$ values of –6‰ to –4‰ are commonly observed among many different groups of carbonaceous chondrites, which would have formed in relatively anhydrous conditions in the protoplanetary disk. Similarly, ungrouped Acfer 094 and CO3.0 Yamato 81020 show bimodal distributions with $\Delta^{17}O$ ~ –5‰ for particles with Mg# > 97 while particles with Mg# < 97 have $\Delta^{17}O$ ~ –2‰.

The combination of mineralogy, chemistry and O isotopes can help constrain the sources of crystalline silicates in the protoplanetary disk, and in particular the comparison of the Mg#-$\Delta^{17}O$ trend in 81P/Wild 2 particles with those of chondrules in various groups of chondrites. One possibility is that 81P/Wild 2 particles derived from silicates that migrated from the inner disk, either by radial diffusion (Ciesla, 2007), or by advection during the initial disk spreading (Yang and Ciesla, 2012). Alternatively, if these silicate particles crystallized beyond asteroid-forming regions, their data would reveal the variety of oxygen isotope reservoirs and/or redox states in the outer solar system. The total number of high precision oxygen isotope analyses on Stardust grains is still limited (<25) and spread over a large range of Mg# (99-60). Thus, more analyses are required to further explore links and differences between cometary and chondritic materials. Nakashima et al. (2012) show that there are some similarities between 81P/Wild 2 particles and CR chondrite chondrules. For instance, FeO-poor 81P/Wild 2 objects show $\Delta^{17}O$ of ~ –2‰ while FeO-rich 81P/Wild 2 objects show $\Delta^{17}O$ from –2‰ to +2‰. However, several CR chondrite chondrules have Mg#'s > 97 with $\Delta^{17}O$ values of ~−2‰ to –6‰, and particles with these characteristics have not been found in 81P/Wild 2. Moreover, CR chondrite chondrules are dominated by those with high Mg#'s (type I), which is much different from the broader distribution

115 of Fo contents in olivine as reported by Frank et al. (2014). It is thus not clear if the ferromagnesian
116 81P/Wild 2 particles are truly related to CR chondrite chondrules, and/or other carbonaceous
117 chondrites.

118 In addition to the lack of Mg#>97 particles without ^{16}O-rich signatures (e.g. $\delta^{17,18}O \sim -$
119 50‰), there are limited amounts of Stardust particle data in the Mg# 80-95 range, including no
120 data from those having Mg#'s between 89 and 94 (Nakamura et al., 2008; Joswiak et al., 2012;
121 Nakashima et al., 2012; Frank et al., 2014). We thus selected five new olivine and pyroxene
122 particles with Mg# >80. The $\Delta^{17}O$ values of these particles should test if the particles are related
123 to refractory silicates (≤–20‰), or chondrule-like silicates from carbonaceous and ordinary
124 chondrites (~ –6 per mil to ~ +2 per mil).

125 To measure the O-isotope ratios, techniques for small spot analysis by secondary ion mass
126 spectrometry (SIMS) are employed (Nakashima et al., 2011, 2012). In a previous study at the
127 WiscSIMS laboratory, Nakashima et al. (2012) successfully analyzed 81P/Wild 2 particles as
128 small as ~ 4 μm by using FIB (Focused Ion Beam) marking and ^{16}O ion imaging. However, due
129 to the limited 1 μm resolution of both stage motion and primary beam deflectors, the aiming was
130 not highly accurate as small deviations between FIB marks and ion probe pits by as much as 0.5
131 μm were observed. For more accurate aiming, we made in-house modifications to the primary
132 beam deflector and developed a new computer-programmable system called the "Nano-deflector",
133 which enables deflecting the primary beam with 0.1μm increments.
134

135 **2. Analytical procedures**

136

137 2.1. Sample Preparation

Seven particles collected from comet 81P/Wild 2 were allocated by CAPTEM (Curation and Analysis Planning Team for Extraterrestrial Materials). To extract the particles from the Stardust spacecraft aerogel, each impact track was carefully cut out and divided into several slabs. Each slab contained a single particle. Five particles come from track 149 (Tona) from 5 distinct slabs (A, E, G, M, P) while two particles are from slab B and C of track 172 (Wawa). The particles, ranging in size from 5 to 15 μm, are mounted in acrylic resin and ultramicrotomed for transmission electron microscope (TEM) analyses. They are selected for SIMS analyses because TEM analyses revealed that they contain coarse (>2 μm) olivine and low-Ca pyroxene with compositions of either high Mg# (≥95) or Mg# ~85.

The particles remaining in the resin were extracted as a 100 μm wide acrylic cubes. Each cube was then pressed into a 1.4 mm diameter indium metal pool centered in an 8 mm aluminum disk, along with a San Carlos olivine standard (Nakashima et al., 2012). The accuracy of oxygen isotope analyses is highly dependent on the flatness of the sample surface, as even slight topography might cause a change in instrumental mass fractionation (Kita et al., 2009). To minimize the topography effects caused by sample holder edges, we used sample holders made of three 8 mm holes (Nakashima et al., 2011, 2012), allowing particles and standards to be positioned within 0.7 mm of the center of the mount.

2.2. Transmitted Electron Microscope Analysis

Microtome sections of the samples were prepared for TEM at the University of Washington by cutting serial slices ~70 nm thick with a Leica Ultracut S ultramicrotome and placing them onto Au or Cu TEM grids containing 10 nm carbon films. They were placed into a double-tilt low-background Be sample holder which was inserted into a Tecnai 200 keV field emission TEM. The

TEM is equipped with a CCD camera for bright- and dark-field imaging and secondary electron and high angle annular dark-field STEM detectors. Energy dispersive X-ray (EDX) spectra were acquired with an EDAX light element X-ray detector and quantified with EDAX Genesis software using standard thin-film k-factors obtained from natural minerals and the NIST SRM2063a thin-film standard. Spectral energy calibration was done using a Cu and Al thin-film prepared at the University of Washington. Maximum relative errors are estimated at 5% for major elements and 25 – 30% for most minor elements. High resolution lattice fringe images and electron diffraction patterns were obtained on some of the minerals to confirm atomic structures. Calibration of high resolution images was done using well-known mineral standards and an Al-thin film for diffraction camera lengths.

2.3. FIB-marking

Backscattered electron (BSE) images of the seven particles were obtained, prior to SIMS analyses, using a scanning electron microscope (SEM, Hitachi S3400) at the University of Wisconsin-Madison. Because the acrylic resin surrounding the sample is sensitive to alteration caused by electron beam damage, acquiring images can create depressions around the sample, and the infliction of surface topography might affect the instrumental mass fractionation during SIMS analyses (Kita et al., 2009). We minimized damage to the acrylic near the sample area by spending as little time as possible on the sample area at high magnification, while focusing BSE images on a region of the acrylic away from the comet particle. The positioning of targeted SIMS analysis regions for each grain was determined according to the BSE images. We used a Zeiss focused ion beam (FIB) field emission (FE)-SEM Auriga (UW-Madison) to mark the SIMS analysis positions by removing a 1 μm x 1 μm square of the carbon coating (SOM A). A focused Ga^+ beam with an

184 accelerating voltage of 30 keV operated with a 5 pA beam current. A series of tests, previously
185 performed, allowed us to determine that the right dosage to remove the 20-nm-thick carbon coating
186 completely without sputtering the surface of the particle was 0.4 nC/ μm^2 (equivalent to 90 seconds
187 of sputtering with our settings). Previous test analyses showed no significant difference between
188 standard analyses with or without FIB marks (Nakashima et al., 2012), so we did not apply FIB
189 marks on any of the standard grains.
190 Prior to SIMS analysis, the topography of samples was checked to confirm that the SEM
191 imaging did not alter the surface significantly. Profilometer images revealed that SEM imaging
192 did not depress the acrylic surface by more than 1 μm around the comet particles.
193
194 2.4. Oxygen isotope analyses
195 Oxygen three-isotope ratios of the seven 81P/Wild 2 particles were acquired with the
196 Cameca IMS 1280 ion microprobe at the WiscSIMS laboratory of the University of Wisconsin-
197 Madison over two analytical sessions. The analytical conditions were similar to those in
198 Nakashima et al. (2012). The primary Cs^+ beam was set at an intensity of 3 pA and beam size of
199 ~1.5 μm in diameter.
200 Prior to each unknown sample analysis, secondary $^{16}O^-$ ion images were obtained in order
201 to identify the FIB marks using 10 μm x 10 μm primary beam rastering (Nakashima et al., 2012).
202 Due to the absence of carbon coating, the FIB marks appear as bright spots, allowing for easy
203 centering of the mark to the image by first adjusting the stage, and then refining the centering with
204 the NanoDeflector. Thanks to the recent addition of the NanoDeflector to the WiscSIMS IMS
205 1280, the adjustment of primary beam positioning (See SOM B for details) was greatly improved
206 and the ion images were centered with a precision of 0.1 μm. We note that Nakashima et al. (2012)

used a smaller primary beam (≤1 μm, 1 pA) for ion imaging to identify the FIB-mark, followed by a 3 pA beam condition (2 μm × 1 μm spot) for the isotope analysis. However, applying two different primary beam conditions between ion imaging and isotope analyses could potentially introduce a sub-μm level inaccuracy for the final sample aiming. The reason why the smaller beam was used for ion imaging is to obtain sharp images, to enable precise aiming (Nakashima et al. 2012). But even with 3pA & 1.5μm beam (this study), ion images were as sharp. Therefore, we used the same primary beam setting for ion imaging and for isotope analyses (3 pA, 1.5 μm). The centering of FIB mark by ion imaging took less than 5 min, and the removal of surface carbon coating was minimal. On two samples (T149/F7 and T172/F3), the FIB-marks were improperly adjusted due to a malfunction of the FE-SEM (Fig. SOM A). However, comparison between SEM images and SIMS ion images of misaligned FIB marks and the precision of the NanoDeflector aiming allowed us to locate SIMS analyses positions correctly (Fig. 1) without having to remove the coating and redo the FIB marks.

Secondary ions $^{16}O^-$, $^{17}O^-$, and $^{18}O^-$ were detected simultaneously on the multicollection system; $^{16}O^-$ by a Faraday cup (typical count rate ~1.6 x10^6 cps, with a background noise of ~1 x10^3 cps (2σ)) and $^{17}O^-$ and $^{18}O^-$ by electron multipliers (EM). The mass resolving power (MRP at 10 % peak height) was set at ~ 6000 for ^{17}O and ~2200 for ^{16}O and ^{18}O. The contribution of tailing $^{16}O^1H^-$ ions on the $^{17}O^-$ signal was negligible (< 0.1 ‰). Each analysis last 20 minutes, giving a typical internal precision of 1.2‰, 2.5‰ and 2.6‰ (2σ) for $\delta^{18}O$, $\delta^{17}O$, $\Delta^{17}O$, respectively.

One to six analyses were performed on each particle, bracketed by eight analyses performed on San Carlos olivine (Fo_{89}) grains mounted in the same disks, within 500 μm of the sample particle. The external reproducibility is calculated as twice the standard deviation (2σ) on the eight standard analyses bracketing the sample analyses, which represent spot-to-spot

reproducibility and is assigned as uncertainty of individual analyses (Kita et al. 2009; Nakashima et al. 2012). They are generally very similar to the internal error of individual analyses, which is determined by FC detector background drift and counting statistics of minor isotopes using EM detectors, as well as a small drift of mass dependent fractionation with increasing analysis depth (Kita et al. 2009, 2010). The analytical uncertainty assigned to single spot analyses is calculated as the mean of the 2σ calculated for each set of the standard measurement brackets over the whole session. For samples with multiple measurements, we obtained the mean values. The uncertainty of the mean values is assigned as the propagation of (1) the maxima of the 2SD of sample data versus the analytical uncertainty of a single analysis, of which this value is divided by the square root of the number of analyses; (2) the 2SE (standard error of the mean) of the instrumental bias calculated from bracket standard analyses, and (3) uncertainties of instrumental mass-dependent fractionation across a 1 mm diameter of the 8 mm sample disk (0.5‰ in $\delta^{18}O$; Nakashima et al., 2012). The same error estimates of average values have been applied to SIMS chondrule analyses in previous studies (Ushikubo et al., 2012; Tenner et al. 2013, 2015). If only one analysis was made for a particle, we propagated uncertainties from (2) and (3) to the final value. The global external reproducibility of the running standards over the whole session was 1.4‰, 2.2‰, and 2.2‰ (2σ) for $\delta^{18}O$, $\delta^{17}O$, $\Delta^{17}O$, respectively. Instrumental biases of olivine and pyroxene were calibrated using multiple standards (Fo_{60}, Fo_{89}, and En_{85} and En_{97}) with known oxygen isotope ratios that cover the range of compositions of the unknowns. Two geological glass standards (75.6 % and 58.6 % SiO_2) were also analyzed, to be used to correct for instrumental bias of unknown analyses in case it inadvertently overlapped with adjacent silica-rich glass (76.0 % SiO_2). These data are reported in Table SOM C.

3. Results

3.1. Petrography and mineral chemistry

Track 149 is a ~4mm-long bulbous track (Burchell et al., 2008) which is composed of a broad cavity, a long narrow root containing the terminal particle (T149/F1) and two short side roots containing fragments T149/F2 and T149/F3. Fragments T149/F6 and T149/F7 were located in the cavity near the base of the bulb. Track 172 is a ~ 0.9 mm-long bulbous track with a distinct narrow root containing the terminal particle. Fragments 2 (T172/F2) and 3 (T172/F3) were present at the termini of shorter side roots emanating from the bottom of the bulb and from the side of the main root, respectively. Major element compositions of microtome sections of the T149 and T172 particles are reported in Table 1. T149/F1 is a 10 × 13 μm olivine grain with a Mg# = 84.6, very similar to particle T149/F3 which is a 5 × 8 μm olivine grain with a Mg# of 86.0. Neither grains have a measurable amount of Al_2O_3. T149/F2 is a 7 × 12 μm pyroxene crystal with a Mg# = 99.5 ($En_{98.3}Wo_{1.2}$). T149/F6 is a 4 × 6 μm pyroxene grain accompanied by a small 1 × 2 μm glass phase. The Mg# of the pyroxene grain is of 94.7 ($En_{92.1}Wo_{2.7}$). T149/F2 contains slightly more Al_2O_3 than T149/F6 (1.61 wt% vs. 1.11 wt% respectively), and contains significantly less Cr_2O_3 (0.50 wt% vs. 1.24 wt%), FeO (0.35 wt% vs. 3.29 wt%) and MnO (0.08 wt% vs. 1.76 wt%) and moderately less CaO (0.63 wt% vs. 1.33 wt%). T149/F7 is a 5 × 7 μm fragment composed entirely of glass with an approximate enstatite composition (Mg# = 96.5). Finally, particles T172/F2 and T172/F3 are Mg# = 99.0 pyroxene grains ($En_{98.9}Wo_{0.1}$ and $En_{99}Wo_{0.3}$, respectively) with sizes of 5 × 9 μm and 4 × 5 μm, respectively. However, T172/F2 is distinctively more depleted in minor oxides (T172/F2: CaO = 0.04 wt%; T172/F3: Al_2O_3 = 0.52 wt%, CaO = 0.15 wt%).

3.2. Oxygen isotopes

A total of 155 analyses were collected over two sessions for a total of 14 analyses on Stardust grains. After the SIMS sessions, we inspected all analysis pits (on Stardust particles and San Carlos olivine standards) by SEM for irregularities and possible overlaps. SIMS aiming was highly accurate, with each pit covering its original FIB mark. No analysis points were rejected. In particular, a close inspection of particle T149/F6 containing glass, which was the most critical aiming-wise, revealed no overlap of pits with the glass phase or the aerogel. For all particles, the SIMS pits were located within < 0.2 μm of their FIB-marks (Fig. 1), or at their intended locations within particles T149/F7 and T172/F3.

Oxygen isotope ratios of the seven particles are given in Table 2 and plotted in Fig. 2, reported as $\delta^{17,18}O = [(R_{sample}/R_{VSMOW}) - 1] \times 1000$; $R = {}^{17,18}O/{}^{16}O$ (VSMOW = Vienna Standard Mean Ocean Water). Oxygen isotope ratios vary from –52.5‰ to 6.6‰ in $\delta^{18}O$ and are distributed along a slope 1 line, as previous 81P/Wild 2 studies have shown (McKeegan et al., 2006; Nakamura et al., 2008; Nakamura-Messenger et al., 2011; Bridges et al., 2012; Ogliore et al., 2012, 2015; Nakashima et al., 2012; Joswiak et al., 2014; Gainsforth et al., 2015). We use the Primitive Chondrule Minerals (PCM) line for reference (Ushikubo et al., 2012), though our analytical precision does not resolve data from the CCAM (Carbonaceous Chondrite Anhydrous Mineral; Clayton et al., 1977) or Young and Russell (1998) lines. Three particles, T149/F1, T149/F2, and T172/F2, have data from multiple SIMS measurements. For T149/F1 and T172/F2, the data are indistinguishable within per-analysis uncertainties in $\delta^{18}O$ and $\delta^{17}O$. T149/F2 has two data points that differ by significantly more than the per-analysis uncertainties in $\delta^{17}O$ and $\Delta^{17}O$, and the uncertainties of the average reflect this.

As shown in Fig. 2, the particles extracted from track 149 all have ^{16}O-poor compositions on a three-isotope plot, with δ^{18}O varying from –8.1 ± 1.2‰ (T149/F2) to +6.6 ± 1.5‰ (T149/F3), while Δ^{17}O varies from –6.9 ±4.2‰ (T149/F2) to +0.6 ± 2.4‰ (T149/F3). In contrast, the pyroxene grains from track 172 show significant enrichment in ^{16}O, with T172/F2 showing a δ^{18}O of –51.2 ± 1.5‰ and a Δ^{17}O of –22.3 ± 1.8‰ while T172/F3 displays a δ^{18}O of –43.0 ± 1.3‰ and a Δ^{17}O of –21.3 ± 2.3‰. This enrichment is of the same order as other ^{16}O-rich particles found in 81P/Wild 2 particles (McKeegan et al., 2006; Nakamura et al., 2008; Nakashima et al., 2012).

4. Discussion

As the particles analyzed from track 149 have ^{16}O-poor signatures, while the two particles from track 172 have ^{16}O-rich characteristics, we discuss particles from tracks 149 and 172 separately below, due to their significant differences in oxygen isotope ratios.

4.1. Relationship between Mg# and Δ^{17}O

Comet 81P/Wild 2 data from ^{16}O-poor ferromagnesian silicates show a correlation between Δ^{17}O and Mg#, with Δ^{17}O increasing as a function of decreasing Mg#, over a rather large range of Δ^{17}O (~–8‰ to ~+3‰; Fig. 3). Among chondrules in primitive chondrites, three main trends are observed: (1) in ordinary chondrites , Δ^{17}O remains nearly constant for most chondrules over the whole Mg# range, with an average of 0.5± 0.9‰ (2σ) except for rare ^{16}O-rich examples (Kita et al., 2010). (2) Ushikubo et al. (2012) showed that chondrules from the ungrouped type 3.0 carbonaceous chondrite Acfer 094 display two distinguishable oxygen isotope sub-groups, likely coming from two distinct oxygen isotope reservoirs: one chondrule sub-group is relatively ^{16}O-

rich with a $\Delta^{17}O = -5.4 \pm 1.2‰$ (2σ) and Mg#'s > 96, and the other group is relatively ^{16}O-poor, with $\Delta^{17}O = -2.2 \pm 0.7‰$ (2σ) and Mg#'s of ~ 99-42. Similarly, Tenner et al. (2013) reported two distinct oxygen isotope groups among chondrules from the CO3.0 chondrite Yamato 81020: A "–5.5‰" chondrule group, showing $\Delta^{17}O$ varying from –4.8‰ to –6.5‰ for Mg#'s >97 and a "–2.5‰" group displaying $\Delta^{17}O$ values of –2.1‰ to –3.0‰ for Mg#'s of ~ 96-36. (3) Among CR chondrites, Tenner et al. (2015) reported monotonic increases in $\Delta^{17}O$ with decreasing Mg# in type I chondrules (Mg# = 99 to 94), from $\Delta^{17}O$ values of −5.9‰ to −1‰, while type II chondrules show variable $\Delta^{17}O$ of −2‰ to +1‰ (Connolly and Huss, 2010; Schrader et al., 2013). For carbonaceous chondrites, the $\Delta^{17}O$ remains nearly constant for moderate Mg# chondrules (< 96, type II), with an average value of 0.0 ± 2.0‰ (2σ) among those from CR chondrites (Connolly and Huss, 2010; Schrader et al., 2013; Tenner et al., 2015), and –2.2 ± 1.3‰ (2σ) among those from CO chondrite Yamato 81020 (Tenner et al., 2013) and the ungrouped Acfer 094 (Ushikubo et al., 2012). The $\Delta^{17}O$ values of high Mg# (Mg# ~96-99) chondrules are much lower than the above, with an average of –5‰. Tenner et al. (2015) hypothesized that the general trend of increasing chondrule $\Delta^{17}O$ with decreasing Mg# in most carbonaceous chondrite groups was caused by mixing between reduced anhydrous dusts ($\Delta^{17}O$: –6‰) and ^{16}O-poor H_2O ice (>0‰) in the chondrule-forming region of the protoplanetary disk, along with variable dust to gas ratios.

In the case of 81P/Wild 2 particles, all but one FeO-poor particle (Mg# >97) show $\Delta^{17}O$ values of ~ –2‰ and FeO-rich particles (Mg# <97) vary between –4‰ and +2‰ (Fig. 3). We ran a series of statistical tests to determine which chondrite group had the most similar $\Delta^{17}O$ and Mg# distribution as 81P/Wild 2. The Kolmogorov-Smirnov test is a statistical test that compares the distributions of two sets of data (or one or two variables each). The p-value parameter translates how close the distributions are: a positive p-value means the distributions are similar, while a p-

344 value ≈ 0 means that the distributions are distinct. The Kolmogorov-Smirnov test for one variable
345 shows that the distribution of 81P/Wild 2 grains $\Delta^{17}O$ (mean = –1.8‰, σ = 2.1‰) is very close to
346 the distribution of $\Delta^{17}O$ measured in CR chondrites chondrules (mean = –2.3‰, σ = 1.8‰) giving
347 a p-value = 0.24, while it is clearly different from the $\Delta^{17}O$ distribution measured in OC chondrules
348 (mean = –0.3‰, σ = 1.6‰) as well as chondrules from both Acfer 094 and Yamato 81020 (mean
349 = –4.0‰, σ = 1.7‰) with a p-value ≈ 0 in both cases. The agreement among the range and
350 variations between CR chondrites chondrule and 81P/Wild 2 grains suggests common precursor
351 characteristics, including the mixing ratios between ^{16}O-poor water ice and ^{16}O-poor dust (Tenner
352 et al., 2015). Tagish Lake-like chondrite WIS91600 (Yamanobe et al. 2016) shows a rather close
353 distribution as well (mean = –3.1, SD = 3.1, p-value = 0.03), which indicates a similar precursor
354 origin.

355 In addition to Mg# and O-isotope relationships, there are other indicators that 81P/Wild 2
356 particles and some chondritic materials originated from a common region of the protoplanetary
357 disk. For instance, based on ^{26}Mg and ^{54}Cr isotopes, Van Kooten et al. (2016) showed that metal-
358 rich carbonaceous chondrites (CR, CB and CH) have a distinct signature from inner solar system
359 objects because the former preserved a high fraction of primordial molecular cloud material,
360 suggesting accretion in more outer regions of the solar system, similar to comets.

361 Moreover, similarities of reflectance spectra between Tagish Lake-like chondrites and D-
362 type asteroids (Hiroi et al., 2001) indicate that Tagish Lake-like chondrites derived from the
363 outermost region of the asteroid belt, which could be a likely origin for CR chondrites and
364 81P/Wild 2 particles. Our new data, particularly in Mg# ranges that were previously lacking (Fig.
365 3), further confirms the similarity between 81P/Wild 2 particles and the CR chondrite chondrule
366 Mg#-$\Delta^{17}O$ trend. In particular, our new data point from particle T149/F2, with the highest Mg#

among the five particles (99.5), displays a $\Delta^{17}O$ value of –6.9 ± 4.2‰ (2SD), indicating a reduced ^{16}O-rich end-member in 81P/Wild 2 particles that is similar to that of high Mg# chondrules in most carbonaceous chondrite groups.

If we run a Kolmogorov-Smirnov test for two variables by taking the Mg# distribution into account in addition to the $\Delta^{17}O$ distribution, the results are slightly different. When we consider only FeO-rich grains (Mg# < 90), the test shows that the distribution of 81P/Wild 2 FeO-rich grains (mean $\Delta^{17}O$ = –1.5 ± 2.4 ‰; 1σ) in Mg# and $\Delta^{17}O$ is the most similar to WIS91600 ($\Delta^{17}O$ = –0.7 ± 1.5 (1σ), p-value = 0.15), is relatively close to CR chondrites ($\Delta^{17}O$ = 0.0 ± 1.0 (1σ), p-value = 0.03), and doesn't fit an OC distribution ($\Delta^{17}O$ = 0.4 ± 0.3 (1σ), p-value ≈ 0), nor the distribution of Acfer 094 and Yamato 81020 ($\Delta^{17}O$ = –2.3 ± 0.6 (1σ), p-value ≈ 0). Perhaps more concerning is that, when considering type I grains, the test shows that those from 81P/Wild 2 do not match any distributions from other chondrites. In particular, the Mg#s of 81P/Wild 2 type I grains are slightly lower (mean Mg# = 96.1 ± 1.65 (1σ)) than those from other groups (Mg# = 98.0 ± 0.93 for CR; Mg# (Yamato 81020 + Acfer 094) = 98 ± 1.9; Mg# (WIS91600) = 99.1 ± 0.33, all 1σ). In addition, CR chondrites are dominated by high Mg# silicates (type I chondrules) which represent ~99 % of the total chondrule population (Weisberg et al., 1993) and ~70 % of 5-30 μm olivine particles studied by Frank et al. (2014). In contrast, the 81P/Wild 2 particles with Mg# > 90 only represent a minority among silicate grains (Frank et al., 2014, estimated a fraction of 22%). This implies that, while the 81P/Wild 2 grains originated from a similar environment as that which produced chondrule silicates from CR chondrties, it was not identical. Specifically, 81P/Wild 2 grains formed in an environment generally more oxidized than that of CR chondrite chondrules, based on metal-silicate equilibria.

389 It is important to note that the Mg# distribution among 81P/Wild 2 particles we investigated
390 is not fully representative of all collected samples. Indeed, particles were purposely selected in an
391 effort to cover the widest possible range of Mg#. Such selection most likely overrepresented the
392 amount of type I particles, which are more critical to our study, compared to type II particle
393 abundances. However, it appears that type I particles show lower Mg#'s than CR chondrite grains,
394 as only 2 out of 8 grains from the ^{16}O-poor cluster have a Mg# above 97, while the large majority
395 (90%) of CR grains type I show a Mg# > 97. According to the model by Tenner et al. (2015), this
396 indicates a dust enrichment of ≈ 300× for 81P/Wild 2 particles, which is slightly higher than the
397 dust enrichment determined for CR chondrites (100-200x).
398
399 Particle T149/F7 is an amorphous grain of enstatite composition. Particles captured in
400 aerogel underwent the peak temperature of ~2000°K for the order of ns to μs (Brownlee et al.,
401 2006). At ~2000°K, the diffusion rate of oxygen isotope in silicate glass is of the order 10^{-4} mm^2/s
402 (Cole and Chakraborty, 2001), which is the equivalent of 10^{-5} μm^2 per ns and too slow to diffuse
403 more than the sub-μm. Therefore, given the rather large dimensions (5×7 μm) of particle T149/F7,
404 it is safe to assume that the core of the grain preserved its pristine isotopic signature. T149/F7
405 shows a Δ^{17}O of 0.5 ± 2.5‰ for a Mg# of 98 (Fig. 3), while the trend suggests that for Mg# of 98,
406 81P/Wild2 particles should show much more negative values (≈ –2‰). Those values place it
407 slightly above the CR chondrite chondrule trend and align it more closely with the ordinary
408 chondrite chondrule trend (Fig 3). Its δ^{18}O and δ^{17}O (respectively 0.7±1.5‰ and 0.8±2.7‰) also
409 place it on or above the TF line, in the domain of ordinary chondrites. Even though the error bars
410 are rather large, these characteristics set it apart from the other 81P/Wild 2 particles. In addition,
411 this particle is an amorphous grain of enstatite composition and is distinctively different to other

412 types of particles in 81P/Wild 2, or other meteoritic analog components. It has been shown that
413 81P/Wild 2 collected different sources of material, and it is probable that T149/F7 came from a
414 reservoir that was distinct from the majority of the 81P/Wild 2 particles which show more similar
415 characteristics to CR chondrite grains.
416
417 4.2. The ^{16}O-rich enstatite particles
418 The pyroxene grains from track 172 show a similar ^{16}O enrichment relative to previous
419 ^{16}O-rich particles found in 81P/Wild 2, such as the CAI Inti (track 25, McKeegan et al., 2006), a
420 relict olivine from chondrule fragment "Gozen-sama" in track 108 (Nakamura et al., 2008), LIME
421 olivine grains from track 57 and 77 (Nakashima et al., 2012), and a forsterite particle from track
422 112 (Nakamura-Messenger et al., 2011). The particles, and in particular T172/F2, contain very
423 little CaO and Al_2O_3 (0.03-0.15% and 0.0-0.5%, respectively; Fig. 4), and are unlikely to be related
424 to CAIs. In chondrules from primitive meteorites, relict olivine and spinel with ^{16}O-rich isotope
425 signatures have been reported (Kunihiro et al., 2004; Wasson et al., 2004; Connolly. and Huss,
426 2010; Ushikubo et al., 2012; Rudraswami et al., 2011; Schrader et al., 2013; Tenner et al., 2013),
427 though significantly ^{16}O-rich enstatites have very rarely been observed. The only occurrence of
428 ^{16}O-rich enstatite has been reported in the matrix of K chondrite Kakangari (Nagashima et al.,
429 2015). Here we propose that ^{16}O-rich and nearly pure enstatite particles from track 172 may have
430 a condensation origin from solar nebula gas, similar to LIME olivine and pure forsterite with ^{16}O-
431 rich isotope signatures.
432 LIME olivines are found in IDPs, the matrices of unequilibrated chondrites (Klöck et al.
433 1989), and AOAs from CR chondrites (Weisberg et al., 2004) and other carbonaceous chondrites
434 (Komatsu et al., 2015). They are considered to have formed by condensation from the solar nebula

435 (Klöck et al., 1989; Ebel et al., 2012). For example, thermodynamic calculations predict that
436 enstatite should condense at the same time as LIME olivine (Ebel et al. 2012). However, Ebel et
437 al. (2012) could not constrain Mn abundances in the condensed enstatite because the partitioning
438 of Mn in enstatite is not known. Joswiak et al. (2012) suggested several nearly pure enstatite
439 particles, showing low contents of Al_2O_3, CaO, TiO_2, Cr_2O_3, and MnO (<1.5% in total), are
440 candidates with possible condensate origins from the solar nebula. Elemental compositions of
441 T172/F2 and T172/F3 match well with these pure enstatite particles (Fig. 4). Including LIME
442 olivines, Joswiak et al. (2012) found that 27 % of 81P/Wild 2 forsterite and enstatite grains (Mg#
443 > 95) have distinct chemical characteristics with very little amounts of minor elements (less than
444 1.5% total oxides such as Al_2O_3, CaO, TiO_2, Cr_2O_3 and MnO). Such compositions suggest a
445 condensation directly from the solar nebula.
446 Joswiak et al. (2012) previously reported a low-Ca pyroxene ($En_{99.8}$; fragment 108 of track
447 77) similar to that from T172/F2 with low total concentrations of Al_2O_3, CaO, TiO_2, Cr_2O_3 and
448 MnO. Although this particular pyroxene grain is too small (≤1 μm) for SIMS oxygen isotope
449 analysis, Nakashima et al. (2012) reported two LIME olivines with $\delta^{18}O \sim -50‰$ among 6 particles
450 from the same track, suggesting possible genetic link between LIME olivine and nearly pure
451 enstatite (T77/F108) among 81P/Wild 2 particles. However, it remains possible that the track 77
452 projectile might have been an aggregate of particles that formed under various environments
453 (Nakashima et al. 2012) that are unrelated.
454 Recently, Messenger et al. (2015) reported a ^{16}O-rich enstatite grain (En_{99}) in a giant cluster
455 chondritic porous IDP. It has a $\delta^{17}O = -40 \pm 9‰$, $\delta^{18}O = -44 \pm 4‰$, and has low abundances of Fe,
456 Cr, and Mn (0.5 wt%, 0.4 wt%, and 0.1 wt%, respectively, similar to those in T172/F2 and
457 T172/F3. Nearly pure enstatites are also observed as whiskers in IDPs, which are believed to have

458 formed by condensation from the nebular gas (Bradley et al., 1983), but they are unfortunately are
459 too small (sub-micron in their smaller dimension) for high precision oxygen three isotope analyses.
460 The rare known occurrences of ^{16}O-rich pyroxenes found in meteorites are those from
461 amoeboid olivine aggregates (AOAs) (Krot et al., 2004), as well as the matrix of CR2 NWA 530
462 (Yurimoto et al. 2004), and K-grouplet chondrite Kakangari (Nagashima et al., 2015) AOAs are
463 aggregates of forsterite olivine, FeNi metal and Ca, Al-rich minerals. They are believed to have
464 formed in the same region as CAIs, but at relatively lower temperatures (Krot et al., 2004). Krot
465 et al. (2004) observed the presence of low-Ca pyroxene in 10 % of AOAs, mostly surrounding
466 olivine grains, which might have formed by reactions involving olivine and surrounding SiO_2 gas.
467 These low-Ca pyroxenes display a ^{16}O enrichment of $\Delta^{17}O < -20$ ‰ (Krot et al., 2005), implying
468 that they formed from the same O-isotope reservoir as the olivine. Alternatively, pyroxene
469 condensates could have formed directly from fractionated gas with Mg/Si ratio lower than that of
470 solar abundance (Krot et al. 2004, 2005). However, even though it is impossible to know with
471 confidence that isolated grains from one track were associated, the presence of LIME olivine grains
472 in track 172 suggests this was the case.
473 Krot et al. (2005) showed that oxygen isotope ratios of low-Ca pyroxene in AOAs becomes
474 ^{16}O-poor as the degree of melting in AOAs increases. They also found that ^{16}O-poor igneous low-
475 Ca pyroxenes contain more refractory elements (CaO, Al_2O_3, and TiO_2), which are not expected
476 to be in the gaseous phase at the condensation temperature of low-Ca pyroxene. As shown in Fig.
477 5, the FeO and MnO contents of T172/F2 and T172/F3 are well within the ranges observed in
478 AOAs (Krot et al. 2004), while Al_2O_3 and CaO contents are at the lowest end compared to those
479 in AOA low-Ca pyroxene (Fig. 4). Krot et al. (2004, 2005) show a correlation between $\Delta^{17}O$ and
480 Al_2O_3 contents in AOA pyroxenes that increase with the degree of melting (Fig. 6). In this regard,

481 the $\Delta^{17}O$ values and the Al_2O_3 contents of particles T172/F2 and T172/F3 are the lowest among
482 AOA-like data, suggesting they represent the unmelted end-member of the pyroxene suite found
483 in AOAs.
484
485 **5. Conclusions**
486 We analyzed oxygen three isotope ratios in seven silicate particles from tracks 149 and 172
487 of comet 81P/Wild 2. Improvement of the WiscSIMS 1280 IMS allowed for us to place the beam
488 on small particles (5-15 μm) using ~1.5 μm spots with an aiming accuracy of 0.1 μm. Particles
489 from track 149 show relatively ^{16}O-poor isotope compositions with $\Delta^{17}O$ values ranging from –
490 2‰ to 0‰, except for one enstatite (En_{99}) with a $\Delta^{17}O$ value of –7‰. These data are similar to
491 those previously observed in 81P/Wild 2 ferromagnesian silicates, but extend the range down to –
492 7‰ with the highest Mg#. These data further confirm a similar $\Delta^{17}O$ and Mg# relationship between
493 81P/Wild 2 particles and CR chondrite chondrules, including the existence of a high Mg# (>98)
494 and low $\Delta^{17}O$ (≤–5‰) component that is commonly observed among chondrules from
495 carbonaceous chondrites. However, FeO-poor (Mg#<90) particles are less abundant in 81P/Wild
496 2 silicates than in CR chondrites, implying that environments of formation for the 81P/Wild 2
497 particles were more oxidized.
498 The two particles from track 172 are the first ^{16}O-rich pyroxenes found among 81P/Wild 2
499 samples, with a $\Delta^{17}O$ of ~ –22‰, or as low as other ^{16}O-rich 81P/Wild 2 particles including LIME
500 olivine. Their oxygen isotopic ratios and elemental compositions are in good agreement with those
501 of pyroxene grains found in AOAs, indicating a link between ^{16}O-rich ferromagnesian silicate
502 particles in 81P/Wild 2 and those in AOAs.
503

Acknowledgements: The authors thank CAPTEM for the allocation of 81P/Wild 2 particles, Richard K. Noll for assistance for FIB and FE-SEM observations, Jim. Kern for SIMS support and profilometer assistance. The authors gratefully acknowledge use of facilities and instrumentation supported by NSF through the University of Wisconsin Materials Research Science and Engineering Center (DMR-1121288). This work is supported by NASA programs (NK: NNX13AD15G, DB: NNX14AF28G). WiscSIMS is partly supported by NSF (EAR03-19230, EAR13-55590).

513 **References**

514

515 Bradley, J.P., Brownlee, D.E., Veblen, D.R., 1983. Pyroxene whiskers and platelets in interplanetary dust:
516 evidence of vapour phase growth. Nature 301, 473–477. doi:10.1038/301473a0
517 Bridges, J.C., Changela, H.G., Nayakshin, S., Starkey, N.A., Franchi, I.A., 2012. Chondrule fragments
518 from Comet Wild2: Evidence for high temperature processing in the outer Solar System. Earth
519 Planet. Sci. Lett. 341–344, 186–194. doi:10.1016/j.epsl.2012.06.011
520 Brownlee, D., Tsou, P., Aléon, J., Alexander, C.M.O., Araki, T., Bajt, S., Baratta, G.A., Bastien, R.,
521 Bland, P., Bleuet, P., Borg, J., Bradley, J.P., Brearley, A., Brenker, F., Brennan, S., Bridges, J.C.,
522 Browning, N.D., Brucato, J.R., Bullock, E., Burchell, M.J., Busemann, H., Butterworth, A.,
523 Chaussidon, M., Cheuvront, A., Chi, M., Cintala, M.J., Clark, B.C., Clemett, S.J., Cody, G.,
524 Colangeli, L., Cooper, G., Cordier, P., Daghlian, C., Dai, Z., D'Hendecourt, L., Djouadi, Z.,
525 Dominguez, G., Duxbury, T., Dworkin, J.P., Ebel, D.S., Economou, T.E., Fakra, S., Fairey,
526 S.A.J., Fallon, S., Ferrini, G., Ferroir, T., Fleckenstein, H., Floss, C., Flynn, G., Franchi, I.A.,
527 Fries, M., Gainsforth, Z., Gallien, J.-P., Genge, M., Gilles, M.K., Gillet, P., Gilmour, J., Glavin,
528 D.P., Gounelle, M., Grady, M.M., Graham, G.A., Grant, P.G., Green, S.F., Grossemy, F.,
529 Grossman, L., Grossman, J.N., Guan, Y., Hagiya, K., Harvey, R., Heck, P., Herzog, G.F., Hoppe,
530 P., Hörz, F., Huth, J., Hutcheon, I.D., Ignatyev, K., Ishii, H., Ito, M., Jacob, D., Jacobsen, C.,
531 Jacobsen, S., Jones, S., Joswiak, D., Jurewicz, A., Kearsley, A.T., Keller, L.P., Khodja, H.,
532 Kilcoyne, A.L.D., Kissel, J., Krot, A., Langenhorst, F., Lanzirotti, A., Le, L., Leshin, L.A.,
533 Leitner, J., Lemelle, L., Leroux, H., Liu, M.-C., Luening, K., Lyon, I., MacPherson, G., Marcus,
534 M.A., Marhas, K., Marty, B., Matrajt, G., McKeegan, K., Meibom, A., Mennella, V., Messenger,
535 K., Messenger, S., Mikouchi, T., Mostefaoui, S., Nakamura, T., Nakano, T., Newville, M.,
536 Nittler, L.R., Ohnishi, I., Ohsumi, K., Okudaira, K., Papanastassiou, D.A., Palma, R., Palumbo,
537 M.E., Pepin, R.O., Perkins, D., Perronnet, M., Pianetta, P., Rao, W., Rietmeijer, F.J.M., Robert,

538 F., Rost, D., Rotundi, A., Ryan, R., Sandford, S.A., Schwandt, C.S., See, T.H., Schlutter, D.,
539 Sheffield-Parker, J., Simionovici, A., Simon, S., Sitnitsky, I., Snead, C.J., Spencer, M.K.,
540 Stadermann, F.J., Steele, A., Stephan, T., Stroud, R., Susini, J., Sutton, S.R., Suzuki, Y., Taheri,
541 M., Taylor, S., Teslich, N., Tomeoka, K., Tomioka, N., Toppani, A., Trigo-Rodríguez, J.M.,
542 Troadec, D., Tsuchiyama, A., Tuzzolino, A.J., Tyliszczak, T., Uesugi, K., Velbel, M., Vellenga,
543 J., Vicenzi, E., Vincze, L., Warren, J., Weber, I., Weisberg, M., Westphal, A.J., Wirick, S.,
544 Wooden, D., Wopenka, B., Wozniakiewicz, P., Wright, I., Yabuta, H., Yano, H., Young, E.D.,
545 Zare, R.N., Zega, T., Ziegler, K., Zimmerman, L., Zinner, E., Zolensky, M., 2006. Comet
546 81P/Wild 2 Under a Microscope. Science 314, 1711–1716. doi:10.1126/science.1135840
547 Burchell, M.J., Fairey, S. a. J., Wozniakiewicz, P., Brownlee, D.E., Hörz, F., Kearsley, A.T., See, T.H.,
548 Tsou, P., Westphal, A., Green, S.F., Trigo-Rodríguez, J.M., Domingúez, G., 2008. Characteristics
549 of cometary dust tracks in Stardust aerogel and laboratory calibrations. Meteorit. Planet. Sci. 43,
550 23–40. doi:10.1111/j.1945-5100.2008.tb00608.x
551 Ciesla, F.J., 2007. Outward Transport of High-Temperature Materials Around the Midplane of the Solar
552 Nebula. Science 318, 613–615. doi:10.1126/science.1147273
553 Clayton, R.N., Onuma, N., Grossman, L., Mayeda, T.K., 1977. Distribution of the pre-solar component in
554 Allende and other carbonaceous chondrites. Earth Planet. Sci. Lett. 34, 209–224.
555 doi:10.1016/0012-821X(77)90005-X
556 Cole, D.R., Chakraborty, S., 2001. Rates and Mechanisms of Isotopic Exchange. Rev. Mineral. Geochem.
557 43, 83–223. doi:10.2138/gsrmg.43.1.83
558 Connolly Jr., H.C., Huss, G.R., 2010. Compositional evolution of the protoplanetary disk: Oxygen
559 isotopes of type-II chondrules from CR2 chondrites. Geochim. Cosmochim. Acta 74, 2473–2483.
560 doi:10.1016/j.gca.2010.01.005
561 Ebel, D.S., Weisberg, M.K., Beckett, J.R., 2012. Thermochemical stability of low-iron, manganese-
562 enriched olivine in astrophysical environments. Meteorit. Planet. Sci. 47, 585–593.
563 doi:10.1111/j.1945-5100.2012.01347.x

564 Frank, D.R., Zolensky, M.E., Le, L., 2014. Olivine in terminal particles of Stardust aerogel tracks and
565 analogous grains in chondrite matrix. Geochim. Cosmochim. Acta 142, 240–259.
566 doi:10.1016/j.gca.2014.05.037
567 Gainsforth, Z., Butterworth, A.L., Stodolna, J., Westphal, A.J., Huss, G.R., Nagashima, K., Ogliore, R.,
568 Brownlee, D.E., Joswiak, D., Tyliszczak, T., Simionovici, A.S., 2015. Constraints on the
569 formation environment of two chondrule-like igneous particles from comet 81P/Wild 2. Meteorit.
570 Planet. Sci. 50, 976–1004. doi:10.1111/maps.12445
571 Greenberg, J.M., Li, A., 1999. Morphological Structure and Chemical Composition of Cometary Nuclei
572 and Dust. Space Sci. Rev. 90, 149–161. doi:10.1023/A:1005298014670
573 Hiroi, T., Zolensky, M.E., Pieters, C.M., 2001. The Tagish Lake Meteorite: A Possible Sample from a D-
574 Type Asteroid. Science 293, 2234–2236. doi:10.1126/science.1063734
575 Joswiak, D.J., Brownlee, D.E., Matrajt, G., Westphal, A.J., Snead, C.J., Gainsforth, Z., 2012.
576 Comprehensive examination of large mineral and rock fragments in Stardust tracks: Mineralogy,
577 analogous extraterrestrial materials, and source regions. Meteorit. Planet. Sci. 47, 471–524.
578 doi:10.1111/j.1945-5100.2012.01337.x
579 Joswiak, D.J., Nakashima, D., Brownlee, D.E., Matrajt, G., Ushikubo, T., Kita, N.T., Messenger, S., Ito,
580 M., 2014. Terminal particle from Stardust track 130: Probable Al-rich chondrule fragment from
581 comet Wild 2. Geochim. Cosmochim. Acta 144, 277–298. doi:10.1016/j.gca.2014.08.017
582 Kita, N.T., Nagahara, H., Tachibana, S., Tomomura, S., Spicuzza, M.J., Fournelle, J.H., Valley, J.W.,
583 2010. High precision SIMS oxygen three isotope study of chondrules in LL3 chondrites: Role of
584 ambient gas during chondrule formation. Geochim. Cosmochim. Acta 74, 6610–6635.
585 doi:10.1016/j.gca.2010.08.011
586 Kita, N.T., Ushikubo, T., Fu, B., Valley, J.W., 2009. High precision SIMS oxygen isotope analysis and
587 the effect of sample topography. Chem. Geol. 264, 43–57. doi:10.1016/j.chemgeo.2009.02.012

588 Klöck, W., Thomas, K.L., McKay, D.S., Palme, H., 1989. Unusual olivine and pyroxene composition in
589 interplanetary dust and unequilibrated ordinary chondrites. Nature 339, 126–128.
590 doi:10.1038/339126a0
591 Komatsu, M., Fagan, T.J., Mikouchi, T., Petaev, M.I., Zolensky, M.E., 2015. LIME silicates in amoeboid
592 olivine aggregates in carbonaceous chondrites: Indicator of nebular and asteroidal processes.
593 Meteorit. Planet. Sci. 50, 1271–1294. doi:10.1111/maps.12460
594 Krot, A.N., Fagan, T.J., Nagashima, K., Petaev, M.I., Yurimoto, H., 2005. Origin of low-Ca pyroxene in
595 amoeboid olivine aggregates: Evidence from oxygen isotopic compositions. Geochim.
596 Cosmochim. Acta 69, 1873–1881. doi:10.1016/j.gca.2004.06.046
597 Krot, A.N., Petaev, M.I., Yurimoto, H., 2004. Amoeboid olivine aggregates with low-Ca pyroxenes: a
598 genetic link between refractory inclusions and chondrules? Geochim. Cosmochim. Acta 68,
599 1923–1941. doi:10.1016/j.gca.2003.10.026
600 Kunihiro, T., Rubin, A.E., McKeegan, K.D., Wasson, J.T., 2004. Oxygen-isotopic compositions of relict
601 and host grains in chondrules in the Yamato 81020 CO3.0 chondrite1. Geochim. Cosmochim.
602 Acta 68, 3599–3606. doi:10.1016/j.gca.2004.02.011
603 Leitner, J., Hoppe, P., Heck, P.R., 2010. First discovery of presolar material of possible supernova origin
604 in impact residues from Comet 81P/Wild 2, in: Lunar and Planetary Science Conference. p. 1607.
605 Matrajt, G., Ito, M., Wirick, S., Messenger, S., Brownlee, D.E., Joswiak, D., Flynn, G., Sandford, S.,
606 Snead, C., Westphal, A., 2008. Carbon investigation of two Stardust particles: A TEM,
607 NanoSIMS, and XANES study. Meteorit. Planet. Sci. 43, 315–334. doi:10.1111/j.1945-
608 5100.2008.tb00625.x
609 McKeegan, K.D., Aléon, J., Bradley, J., Brownlee, D., Busemann, H., Butterworth, A., Chaussidon, M.,
610 Fallon, S., Floss, C., Gilmour, J., Gounelle, M., Graham, G., Guan, Y., Heck, P.R., Hoppe, P.,
611 Hutcheon, I.D., Huth, J., Ishii, H., Ito, M., Jacobsen, S.B., Kearsley, A., Leshin, L.A., Liu, M.-C.,
612 Lyon, I., Marhas, K., Marty, B., Matrajt, G., Meibom, A., Messenger, S., Mostefaoui, S.,
613 Mukhopadhyay, S., Nakamura-Messenger, K., Nittler, L., Palma, R., Pepin, R.O., Papanastassiou,

614 D.A., Robert, F., Schlutter, D., Snead, C.J., Stadermann, F.J., Stroud, R., Tsou, P., Westphal, A.,
615 Young, E.D., Ziegler, K., Zimmermann, L., Zinner, E., 2006. Isotopic Compositions of Cometary
616 Matter Returned by Stardust. Science 314, 1724–1728. doi:10.1126/science.1135992
617 Messenger, S., Brownlee, D.E., Joswiak, D.J., Nguyen, A.N., 2015. Nebular and Interstellar Materials in
618 a Giant Cluster IDP of Probable Cometary Origin. LPI Contrib. 1856, 5365.
619 Messenger, S., Joswiak, D., Ito, M., Matrajt, G., Brownlee, D.E., 2009. Discovery of presolar SiC from
620 Comet WILD-2, in: Lunar and Planetary Science Conference. p. 1790.
621 Nagashima, K., Krot, A.N., Huss, G.R., 2015. Oxygen-isotope compositions of chondrule phenocrysts
622 and matrix grains in Kakangari K-grouplet chondrite: Implication to a chondrule-matrix genetic
623 relationship. Geochim. Cosmochim. Acta 151, 49–67. doi:10.1016/j.gca.2014.12.012
624 Nakamura, T., Noguchi, T., Tsuchiyama, A., Ushikubo, T., Kita, N.T., Valley, J.W., Zolensky, M.E.,
625 Kakazu, Y., Sakamoto, K., Mashio, E., Uesugi, K., Nakano, T., 2008. Chondrulelike Objects in
626 Short-Period Comet 81P/Wild 2. Science 321, 1664–1667. doi:10.1126/science.1160995
627 Nakamura-Messenger, K., Keller, L.P., Clemett, S.J., Messenger, S., Ito, M., 2011. Nanometer-scale
628 anatomy of entire Stardust tracks. Meteorit. Planet. Sci. 46, 1033–1051. doi:10.1111/j.1945-
629 5100.2011.01211.x
630 Nakashima, D., Ushikubo, T., Joswiak, D.J., Brownlee, D.E., Matrajt, G., Weisberg, M.K., Zolensky,
631 M.E., Kita, N.T., 2012. Oxygen isotopes in crystalline silicates of comet Wild 2: A comparison of
632 oxygen isotope systematics between Wild 2 particles and chondritic materials. Earth Planet. Sci.
633 Lett. 357–358, 355–365. doi:10.1016/j.epsl.2012.09.041
634 Nakashima, D., Ushikubo, T., Zolensky, M.E., Weisberg, M.K., Joswiak, D.J., Brownlee, D.E., Matrajt,
635 G., Kita, N.T., 2011. High precision oxygen three isotope analysis of Wild-2 particles and
636 anhydrous chondritic interplanetary dust particles.
637 Ogliore, R.C., Huss, G.R., Nagashima, K., Butterworth, A.L., Gainsforth, Z., Stodolna, J., Westphal, A.J.,
638 Joswiak, D., Tyliszczak, T., 2012. Incorporation of a Late-forming Chondrule into Comet Wild 2.
639 Astrophys. J. Lett. 745, L19. doi:10.1088/2041-8205/745/2/L19

640 Ogliore, R.C., Nagashima, K., Huss, G.R., Westphal, A.J., Gainsforth, Z., Butterworth, A.L., 2015.
641 Oxygen Isotopic Composition of Coarse- and Fine-grained Material from Comet 81P/Wild 2.
642 ArXiv150604783 Astro-Ph.
643 Rudraswami, N.G., Ushikubo, T., Nakashima, D., Kita, N.T., 2011. Oxygen isotope systematics of
644 chondrules in the Allende CV3 chondrite: High precision ion microprobe studies. Geochim.
645 Cosmochim. Acta 75, 7596–7611. doi:10.1016/j.gca.2011.09.035
646 Sandford, S.A., Aléon, J., Alexander, C.M.O., Araki, T., Bajt, S., Baratta, G.A., Borg, J., Bradley, J.P.,
647 Brownlee, D.E., Brucato, J.R., Burchell, M.J., Busemann, H., Butterworth, A., Clemett, S.J.,
648 Cody, G., Colangeli, L., Cooper, G., D'Hendecourt, L., Djouadi, Z., Dworkin, J.P., Ferrini, G.,
649 Fleckenstein, H., Flynn, G.J., Franchi, I.A., Fries, M., Gilles, M.K., Glavin, D.P., Gounelle, M.,
650 Grossemy, F., Jacobsen, C., Keller, L.P., Kilcoyne, A.L.D., Leitner, J., Matrajt, G., Meibom, A.,
651 Mennella, V., Mostefaoui, S., Nittler, L.R., Palumbo, M.E., Papanastassiou, D.A., Robert, F.,
652 Rotundi, A., Snead, C.J., Spencer, M.K., Stadermann, F.J., Steele, A., Stephan, T., Tsou, P.,
653 Tyliszczak, T., Westphal, A.J., Wirick, S., Wopenka, B., Yabuta, H., Zare, R.N., Zolensky, M.E.,
654 2006. Organics Captured from Comet 81P/Wild 2 by the Stardust Spacecraft. Science 314, 1720–
655 1724. doi:10.1126/science.1135841
656 Schrader, D.L., Connolly Jr., H.C., Lauretta, D.S., Nagashima, K., Huss, G.R., Davidson, J., Domanik,
657 K.J., 2013. The formation and alteration of the Renazzo-like carbonaceous chondrites II: Linking
658 O-isotope composition and oxidation state of chondrule olivine. Geochim. Cosmochim. Acta 101,
659 302–327. doi:10.1016/j.gca.2012.09.045
660 Tenner, T.J., Nakashima, D., Ushikubo, T., Kita, N.T., Weisberg, M.K., 2015. Oxygen isotope ratios of
661 FeO-poor chondrules in CR3 chondrites: Influence of dust enrichment and H2O during chondrule
662 formation. Geochim. Cosmochim. Acta 148, 228–250. doi:10.1016/j.gca.2014.09.025
663 Tenner, T.J., Ushikubo, T., Kurahashi, E., Kita, N.T., Nagahara, H., 2013. Oxygen isotope systematics of
664 chondrule phenocrysts from the CO3.0 chondrite Yamato 81020: Evidence for two distinct

665 oxygen isotope reservoirs. Geochim. Cosmochim. Acta 102, 226–245.
666 doi:10.1016/j.gca.2012.10.034
667 Ushikubo, T., Kimura, M., Kita, N.T., Valley, J.W., 2012. Primordial oxygen isotope reservoirs of the
668 solar nebula recorded in chondrules in Acfer 094 carbonaceous chondrite. Geochim. Cosmochim.
669 Acta 90, 242–264. doi:10.1016/j.gca.2012.05.010
670 Van Kooten, E.M.M.E., Wielandt, D., Schiller, M., Nagashima, K., Thomen, A., Larsen, K.K., Olsen,
671 M.B., Nordlund, Å., Krot, A.N., Bizzarro, M., 2016. Isotopic evidence for primordial molecular
672 cloud material in metal-rich carbonaceous chondrites. Proc. Natl. Acad. Sci. 113, 2011–2016.
673 doi:10.1073/pnas.1518183113
674 Wasson, J.T., Rubin, A.E., Yurimoto, H., 2004. Evidence in CO3.0 chondrules for a drift in the O
675 isotopic composition of the solar nebula. Meteorit. Planet. Sci. 39, 1591–1598.
676 doi:10.1111/j.1945-5100.2004.tb00129.x
677 Weisberg, M.K., Connolly, H.C., Ebel, D.S., 2004. Petrology and origin of amoeboid olivine aggregates
678 in CR chondrites. Meteorit. Planet. Sci. 39, 1741–1753. doi:10.1111/j.1945-5100.2004.tb00070.x
679 Weisberg, M.K., Ebel, D.S., Connolly Jr., H.C., Kita, N.T., Ushikubo, T., 2011. Petrology and oxygen
680 isotope compositions of chondrules in E3 chondrites. Geochim. Cosmochim. Acta 75, 6556–
681 6569. doi:10.1016/j.gca.2011.08.040
682 Weisberg, M.K., Prinz, M., Clayton, R.N., Mayeda, T.K., 1993. The CR (Renazzo-type) carbonaceous
683 chondrite group and its implications. Geochim. Cosmochim. Acta 57, 1567–1586.
684 doi:10.1016/0016-7037(93)90013-M
685 Yamanobe M., Nakamura T., Nakashima D., 2016. Oxygen Isotope Ratios of Chondrules and Isolated
686 Forsterite and Olivine Grains in the WIS91600 Carbonaceous Chondrite from D-Type Asteroid,
687 47th Lunar and Planetary Science Conference (2016), Abstract #1861.
688
689 Yang, L., Ciesla, F.J., 2012. The effects of disk building on the distributions of refractory materials in the
690 solar nebula. Meteorit. Planet. Sci. 47, 99–119. doi:10.1111/j.1945-5100.2011.01315.x

691 Young, E.D., Russell, S.S., 1998. Oxygen Reservoirs in the Early Solar Nebula Inferred from an Allende
692 CAI. Science 282, 452–455. doi:10.1126/science.282.5388.452
693 Yurimoto H., Nagashima K and Emori H., 2004. Radial migration of materials from inner to outer solar
694 nebula: Evidence from meteorite matrix. Lunar Planet. Sci. 35, abstract #1649
695 Zolensky, M.E., Zega, T.J., Yano, H., Wirick, S., Westphal, A.J., Weisberg, M.K., Weber, I., Warren,
696 J.L., Velbel, M.A., Tsuchiyama, A., Tsou, P., Toppani, A., Tomioka, N., Tomeoka, K., Teslich,
697 N., Taheri, M., Susini, J., Stroud, R., Stephan, T., Stadermann, F.J., Snead, C.J., Simon, S.B.,
698 Simionovici, A., See, T.H., Robert, F., Rietmeijer, F.J.M., Rao, W., Perronnet, M.C.,
699 Papanastassiou, D.A., Okudaira, K., Ohsumi, K., Ohnishi, I., Nakamura-Messenger, K.,
700 Nakamura, T., Mostefaoui, S., Mikouchi, T., Meibom, A., Matrajt, G., Marcus, M.A., Leroux, H.,
701 Lemelle, L., Le, L., Lanzirotti, A., Langenhorst, F., Krot, A.N., Keller, L.P., Kearsley, A.T.,
702 Joswiak, D., Jacob, D., Ishii, H., Harvey, R., Hagiya, K., Grossman, L., Grossman, J.N., Graham,
703 G.A., Gounelle, M., Gillet, P., Genge, M.J., Flynn, G., Ferroir, T., Fallon, S., Ebel, D.S., Dai,
704 Z.R., Cordier, P., Clark, B., Chi, M., Butterworth, A.L., Brownlee, D.E., Bridges, J.C., Brennan,
705 S., Brearley, A., Bradley, J.P., Bleuet, P., Bland, P.A., Bastien, R., 2006. Mineralogy and
706 Petrology of Comet 81P/Wild 2 Nucleus Samples. Science 314, 1735–1739.
707 doi:10.1126/science.1135842
708
709
710

Figure Captions

Fig. 1. Comet 81P/Wild 2 particles analyzed by SIMS in this study. (a-e, g-h) BSE images of the seven 81P/Wild 2 particles, after SIMS analyses. (a) T149/F1, (b) T149/F3, (c) T149/F2, (d) T149/F6, (e) T172/F2, (g) T149/F7, (h) T172/F3. SIMS pits are clearly visible, in lieu of the FIB-marks. (g) and (h) show the misaligned FIB-marks, still visible at the surface of the grains. (f) Bright field image of particle T149/F6, showing the position of the glass phase.

Fig. 2. Oxygen three-isotope ratios of the seven 81P/Wild 2 particles. TF, Y&R, CCAM and PCM represent the terrestrial fractionation line, the Young & Russell line, the carbonaceous chondrite anhydrous mineral line and the primitive chondrule line, respectively. Literature data from McKeegan et al. (2006), Nakamura et al. (2008), Nakamura-Messenger et al. (2011), Bridges et al. (2012), Ogliore et al. (2012), Nakashima et al. (2012).

Fig. 3: Relationship between Mg# and $\Delta^{17}O$ in ferromagnesian 81P/Wild 2 particles and comparison to those in chondrules in primitive chondrites. Stardust literature data from McKeegan et al. (2006), Nakamura et al. (2008), Nakashima et al. (2012), and Ogliore et al. (2015). Yamato 81020 (CO3) data from Tenner et al. (2013), Acfer 094 (ungrouped C) data from Ushikubo et al. (2012), LL3 chondrite data from Kita et al. (2010), CR chondrite data from Connolly and Huss (2010), Schrader et al. (2013), and Tenner et al. (2015a).

Fig. 4: Comparison between Al_2O_3 and CaO contents in AOAs and 81P/Wild 2 pyroxenes. Literature data are from Nakamura et al. (2008), Joswiak et al. (2012) and Nakashima et al. (2015)

734 for Stardust samples, and Krot et al. (2004) for AOAs. 81P/Wild 2 particles are strongly depleted
735 in Al_2O_3 and CaO compared to AOAs and other Stardust pyroxenes.
736
737 Fig. 5: FeO and MnO contents (Wt%) of low-Ca pyroxenes in 81P/Wild 2 (Nakamura et al. 2008,
738 this study) compared to those in AOAs (Krot et al. 2004). 81P/Wild 2 LIME olivine data (Joswiak
739 et al. 2012) are shown as reference, which plot above MnO/FeO =1 line. Both ^{16}O-rich pyroxenes
740 (T172/F2, T172/F3) plot within a range of pyroxene in AOAs, and significantly below LIME
741 olivines from 81P/Wild 2.
742
743 Fig. 6: Comparison between Al_2O_3 content and $\Delta^{17}O$ in AOAs (Krot et al. 2004) and 81P/Wild 2
744 particle T172/F2 (this study). T172/F2 appears as the end-member of the trend showing that $\Delta^{17}O$
745 and Al_2O_3 content increases with increased AOA degree of melting.
746
747 Table 1: Content in major elements for the seven 81P/Wild 2 particles from track 149 and track
748 172.
749
750 Table 2: Oxygen isotope ratios of the seven 81P/Wild 2 particles obtained on the IMS 1280.
751 Uncertainties are estimated as external reproducibility (2σ).
752
753 SOM A: (a-e) BSE SEM images of the seven 81P/Wild 2 particles, after FIB marking and prior to
754 SIMS analyses. (a) T149/F1, (b) T149/F3, (c) T149/F2, (d) T149/F6, (e) T172/F2, (g) T149/F7,
755 (h) T172/F3. (f) Bright field image of particle T149/F6, showing the position of the glass phase.
756
757 SOM B: NanoDeflector.

758

759 SOM C: Raw SIMS measured oxygen isotope data of the seven 81P/Wild 2 particles.

Table 1: Major element compositions of the seven Wild 2 particles from track 149 and track 172 (normalized oxide wt%).

Track	Slab	sample	Size (um)	SiO_2	Al_2O_3	Cr_2O_3	FeO	MnO	MgO	CaO	Fo	Fs	En	Wo	Mg#
T149	A	T149/F1	18 x 23	39.73	b.d.	0.30	14.53	0.43	44.77	0.25	84.6	-----	-----	-----	84.6
T149	E	T149/F2	7 x 12	60.24	1.61	0.50	0.35	0.08	36.60	0.63	-----	0.5	98.3	1.2	99.5
T149	G	T149/F3	5 x 8	41.24	b.d.	0.42	13.02	0.49	44.68	0.16	86.0	-----	-----	-----	86.0
T149	M	T149/F6	4 x 6	58.50	1.11	1.24	3.29	1.76	32.76	1.33	-----	5.2	92.1	2.7	94.7
T149	P	T149/F7	5x7	63.39	b.d.	0.29	1.25	1.01	34.06	0.00	-----	-----	-----	-----	98.0
T172	B	T172/F2	5 x 9	58.49	b.d.	0.19	0.73	0.15	40.40	0.04	-----	1.0	98.9	0.1	99.0
T172	C	T172/F3	4 x 5	57.86	0.52	0.29	0.57	0.20	40.41	0.15	-----	0.7	99.0	0.3	99.3

b.d. = below detection.

Table 2: Oxygen isotope ratios of the seven Wild 2 particles.

Track	Slab	sample	analyse #	$\delta^{18}O$	2σ	$\delta^{17}O$	2σ	$\Delta^{17}O$	2σ
T149	A	T149/F1	1	3.6	1.3	-0.1	2.2	-1.9	2.5
			2	4.9	1.3	2.7	2.2	0.2	2.5
			3	3.6	1.3	1.3	2.2	-0.5	2.5
			4	4.8	1.3	1.1	2.2	-1.4	2.5
			5	4.5	1.3	-0.4	2.2	-2.8	2.5
			6	4.3	1.3	-1.5	2.2	-3.7	2.5
			average	**4.3**	**0.9**	**0.5**	**1.5**	**-1.7**	**1.5**
T149	E	T149/F2	1	-7.8	1.1	-13.0	2.0	-8.9	1.8
			2	-8.3	1.1	-9.1	2.0	-4.8	1.8
			average	**-8.1**	**1.0**	**-11.0**	**3.9**	**-6.8**	**4.2**
T149	G	T149/F3	1	6.6	1.5	4.0	2.4	0.6	2.4
T149	M	T149/F6	1	-2.1	1.5	-1.4	2.4	-0.3	2.4
T149	P	T149/F7	1	0.7	1.5	0.8	2.7	0.5	2.5
T172	B	T172/F2	1	-52.5	1.7	-50.5	2.5	-23.2	2.7
T172			2	-51.2	1.7	-48.1	2.5	-21.5	2.7
T172			**average**	**-51.9**	**1.5**	**-49.3**	**2.5**	**-22.3**	**2.1**
T172	C	T172/F3	1	-43.0	1.3	-43.6	2.4	-21.3	2.3

Uncertainties (2σ) of individual spot analyses are the same as external reproducibility (2SD) of bracketting standard. See text for error assignments for average values of multiple analyses.

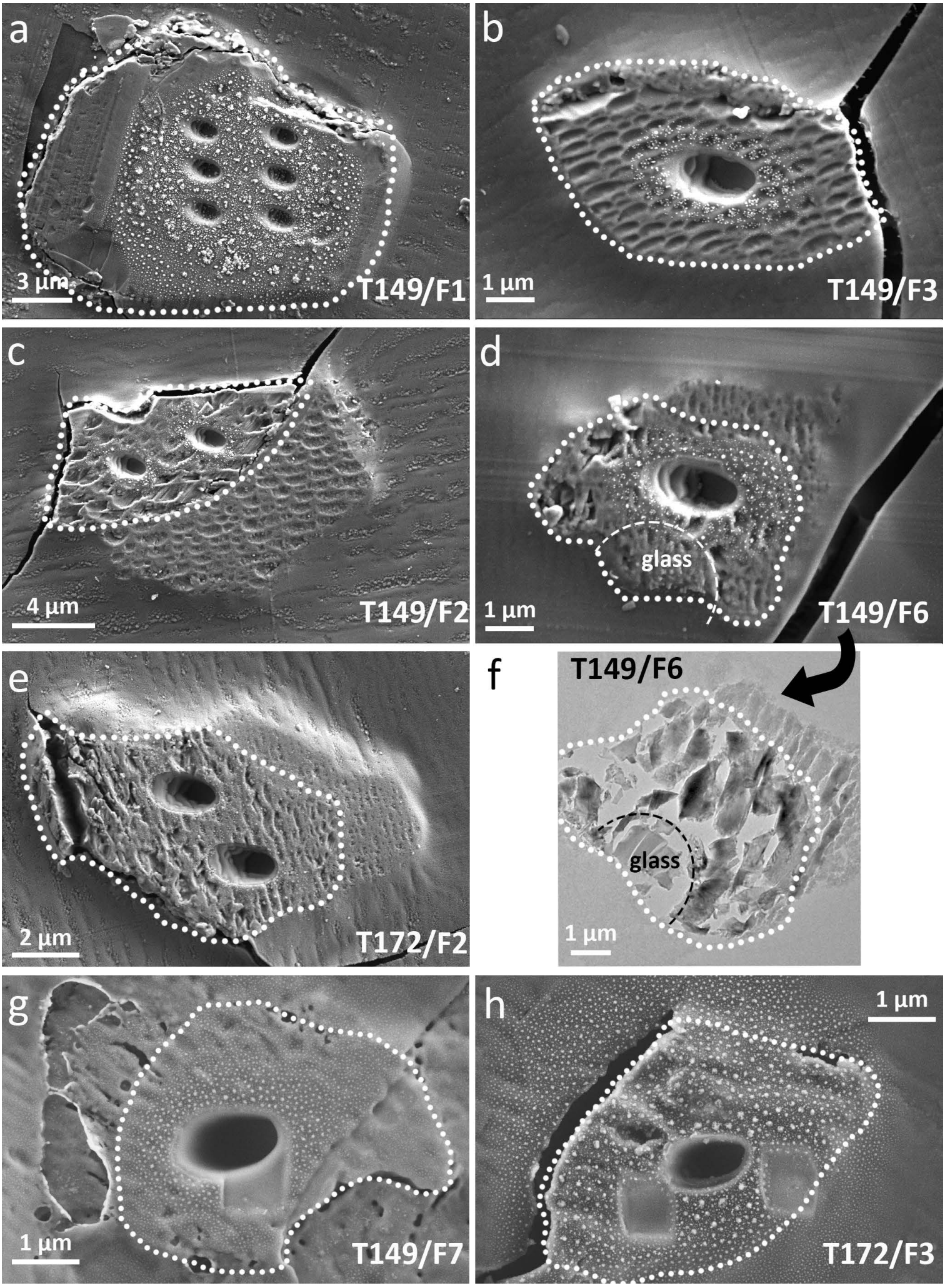
a
3 µm
T149/F1
b
1 µm
T149/F3
c
4 µm
T149/F2
d
glass
1 µm
T149/F6
e
2 µm
T172/F2
f
T149/F6
glass
1 µm
g
1 µm
T149/F7
h
1 µm
T172/F3

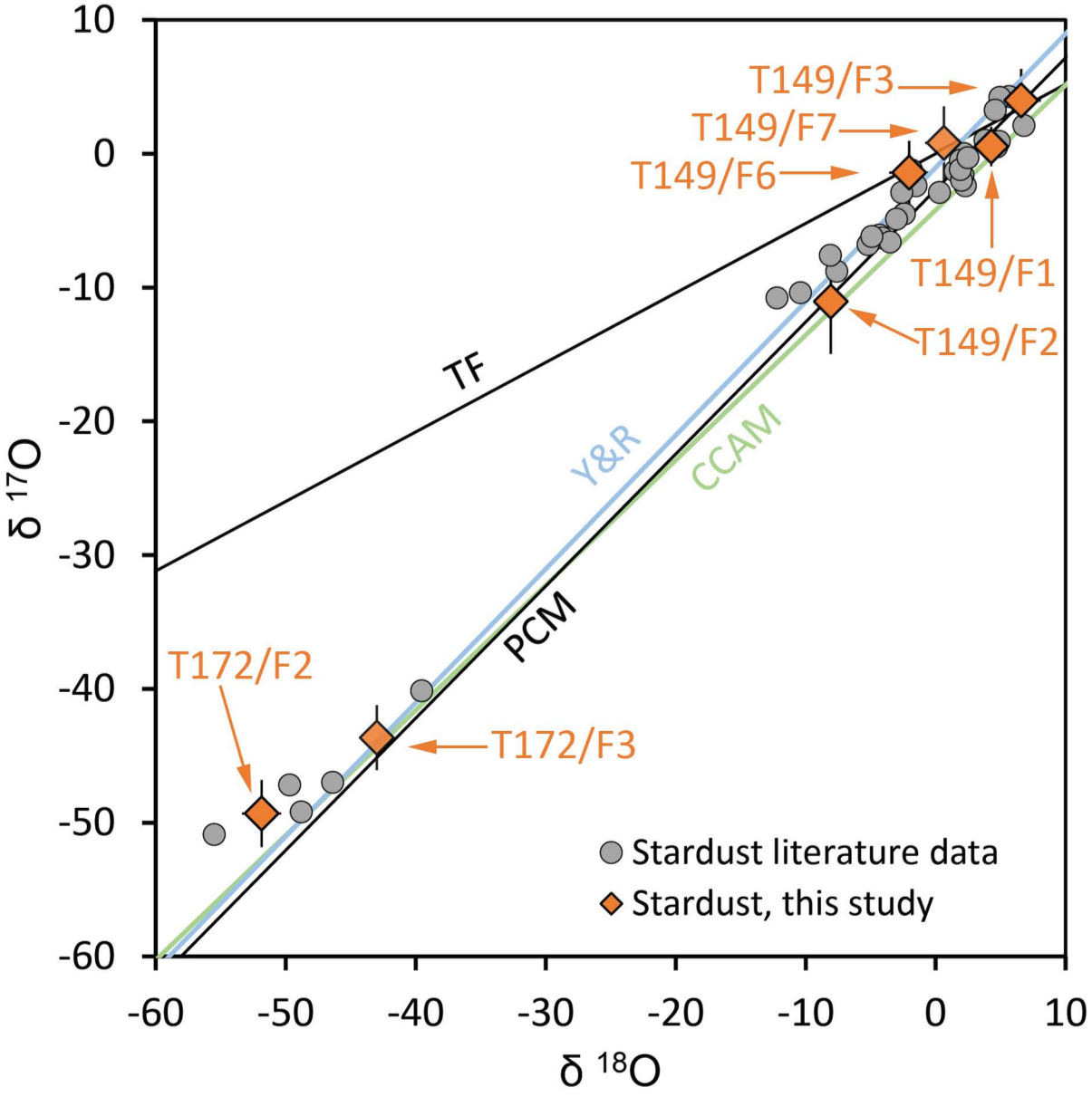
10
0
-10
-20
-30
-40
-50
-60
δ 17O
-60
-50
-40
-30
-20
-10
0
10
δ 18O
T149/F3
T149/F7
T149/F6
T149/F1
T149/F2
T172/F2
T172/F3
TF
Y&R
CCAM
PCM
Stardust literature data
Stardust, this study

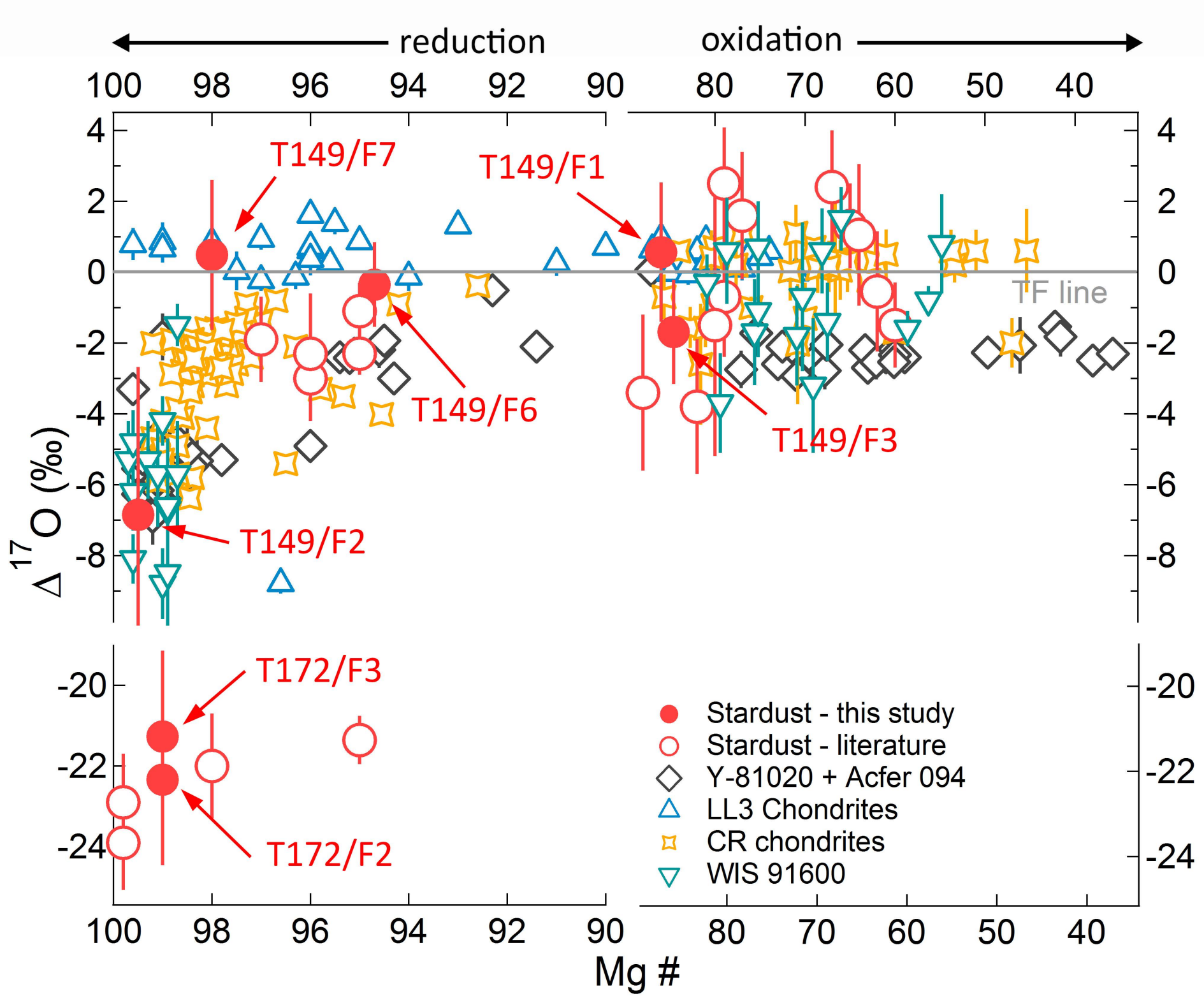
reduction
oxidation
100
98
96
94
92
90
80
70
60
50
40
4
2
0
-2
-4
-6
-8
-20
-22
-24
T149/F7
T149/F1
T149/F6
T149/F3
T149/F2
T172/F3
T172/F2
TF line
Δ17O (‰)
Mg #
Stardust - this study
Stardust - literature
Y-81020 + Acfer 094
LL3 Chondrites
CR chondrites
WIS 91600

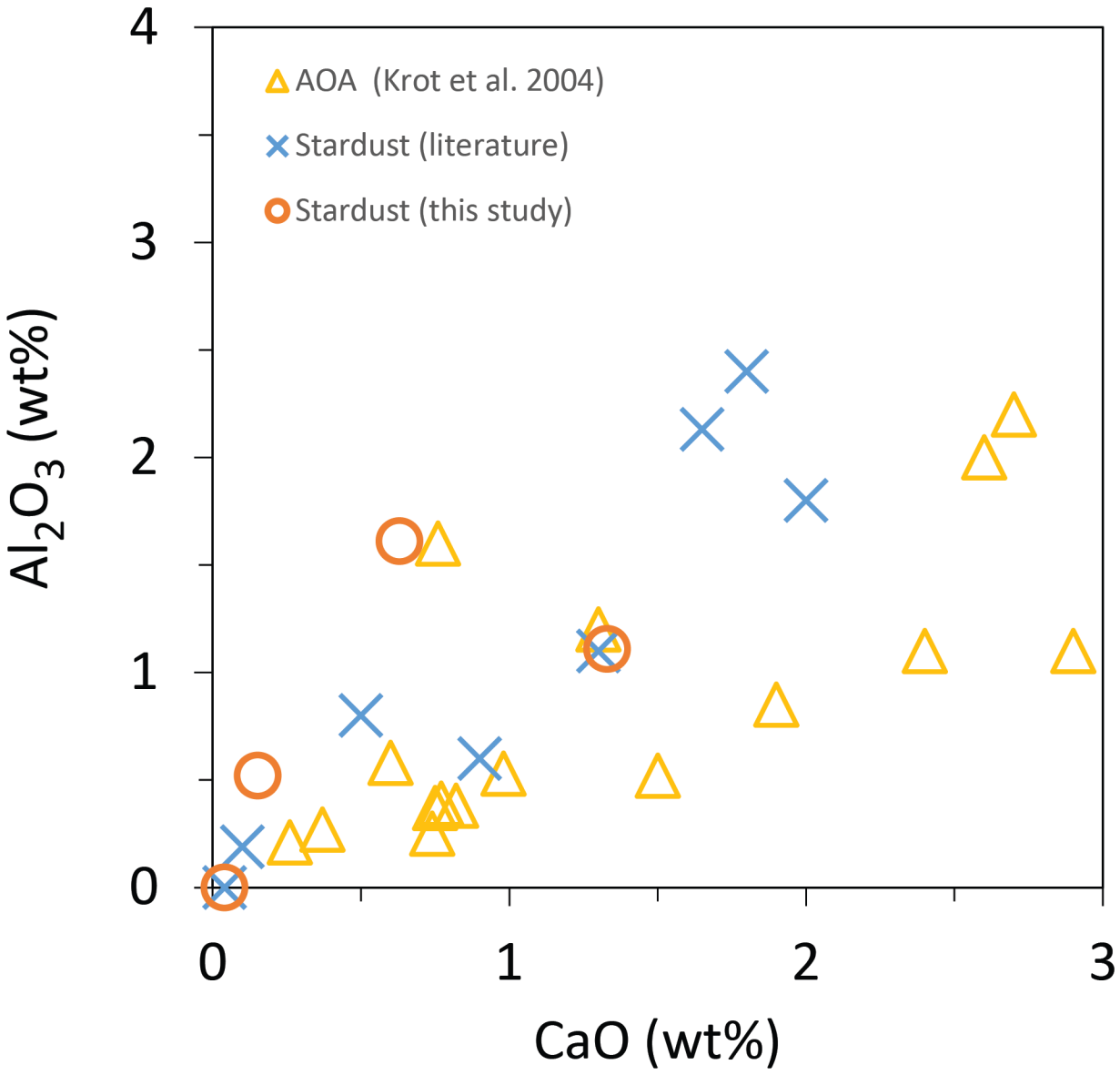
AOA (Krot et al. 2004)
Stardust (literature)
Stardust (this study)
Al2O3 (wt%)
CaO (wt%)
0
1
2
3
4

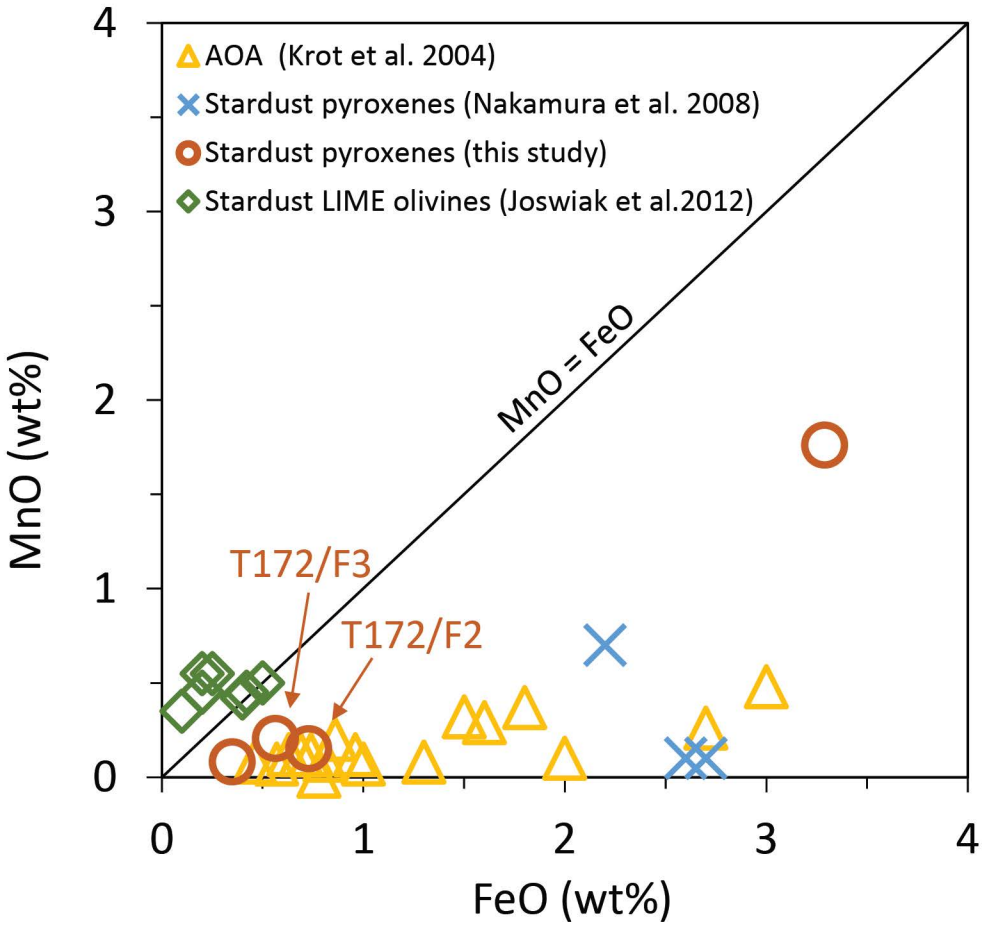
AOA (Krot et al. 2004)
Stardust pyroxenes (Nakamura et al. 2008)
Stardust pyroxenes (this study)
Stardust LIME olivines (Joswiak et al.2012)
MnO = FeO
T172/F3
T172/F2
MnO (wt%)
FeO (wt%)
0
1
2
3
4

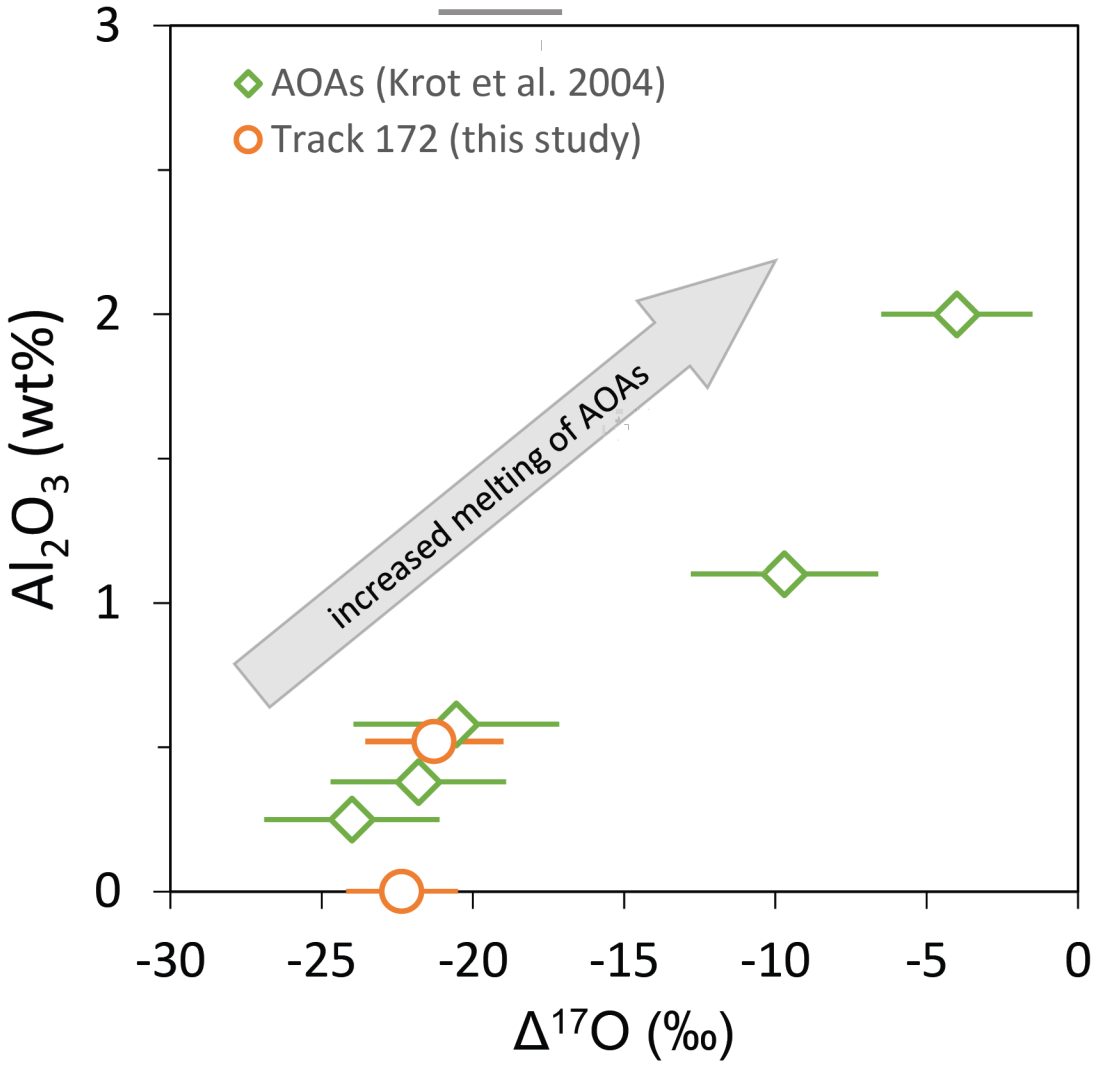
AOAs (Krot et al. 2004)
Track 172 (this study)
increased melting of AOAs
Al_2O_3 (wt%)
$\Delta^{17}O$ (‰)
3
2
1
0
-30
-25
-20
-15
-10
-5
0